QUARTERLY JOURNAL OF THE ROYAL METEOROLOGICAL SOCIETY
Q. J. R. Meteorol. Soc. **136(s1)**: 456–470 (2010)
Published online 18 August 2009 in Wiley InterScience
(www.interscience.wiley.com) DOI: 10.1002/qj.465

Impact of soil moisture on the development of a Sahelian mesoscale convective system: A case-study from the AMMA Special Observing Period

Christopher M. Taylor,[a]* Phil P. Harris[a] and Douglas J. Parker[b]
[a]*Centre for Ecology and Hydrology, Wallingford, United Kingdom*
[b]*University of Leeds, United Kingdom*

ABSTRACT: Interactions between the land and atmosphere play an important role in the precipitation of the Sahel. The African Monsoon Multidisciplinary Analysis Special Observing Period provided observations with which to illuminate potential feedback mechanisms. This case-study highlights a major storm which developed over northern Mali in an area where a research aircraft was surveying the atmospheric response to soil moisture features. Soil moisture variability is characterized using satellite land-surface temperature data whilst cloud images illustrate the evolution of the storm and its relationship to the surface.

Measurements in the planetary boundary layer (PBL) indicate mesoscale variations in pre-storm humidity and temperature consistent with high evaporation from wet soils. The storm developed above a dry surface within a wetter region with cells first appearing along a wet–dry soil boundary. This suggests that the storm was triggered in association with low-level convergence driven by the soil moisture pattern. A gravity wave propagating away from a remote mature storm also appears to have played an important role in the initiation, though only in the region of the soil moisture contrast did deep convection become established. Once organised into a Mesoscale Convective System, convection developed over wet areas as well as dry, and indeed at this stage, convection became more intense over wetter soils. This behaviour is consistent with the large gradients in PBL humidity. The study illustrates the complexity of soil moisture–convection feedback loops and highlights the mechanisms which may operate at different stages of a storm's life cycle.

KEY WORDS land–atmosphere feedback; rainfall; convective initiation

Received 12 December 2008; Revised 7 May 2009; Accepted 28 May 2009

1. Introduction

Many studies have shown a strong sensitivity of the climate of West Africa to the land surface. The region has been identified as a globally important 'hotspot' for feedbacks between rainfall and soil moisture (Koster *et al.*, 2004). Feedbacks between precipitation and the land require strong sensitivities both of the atmosphere to land surface fluxes of heat and water, and conversely, of these surface fluxes to precipitation. In West Africa, the former condition is met during the summer monsoon, when the vast majority of the annual rainfall occurs. The latter condition requires that surface evaporation is limited by soil moisture rather than temperature, radiation or wind. During the monsoon season the Sahel area, lying between the forests to the south and the desert to the north, satisfies the second condition (Gash *et al.*, 1997). The savannah vegetation develops rapidly during the summer in response to precipitation, and this produces a strong seasonal signal in the surface fluxes. Within the wet season, and particularly where the vegetation is sparse, there is very marked day-to-day variation in the surface energy balance arising from direct evaporation in the upper layers of the soil. High rates of evaporation occur for 1 to 2 days after a storm in sandy soils typical of the region.

In global atmospheric models, such as those used by Koster *et al.* (2004), rainfall can be affected by surface fluxes by two routes. During daytime, surface inputs of heat and moisture can directly modify the thermodynamic profile in which convection occurs. Surface fluxes can also influence the regional circulation, which in turn may modify the convective environment through large-scale moisture transport. Following the work of Charney (1975) on desertification, there have been many studies which have investigated large-scale feedback mechanisms in this region. These have looked at the atmospheric response to changes in vegetation cover (e.g. Xue and Shukla, 1993; Zheng *et al.*, 1999; Texier *et al.*, 2000; Clark *et al.*, 2001; Taylor *et al.*, 2002) and the response of the monsoon circulation to variability in vegetation, albedo and soil moisture (Eltahir and Gong, 1996; Ramel *et al.*, 2006; Taylor, 2008).

Global atmospheric models do not have adequate spatial resolution to accurately depict individual storms

*Correspondence to: Christopher M. Taylor, Centre for Ecology and Hydrology, Maclean Building, Crowmarsh Gifford, Wallingford, Oxfordshire, OX10 8BB, UK. E-mail: cmt@ceh.ac.uk

and their associated feedbacks with the land. Mesoscale studies on the other hand can give a clearer picture of the convective response to surface fluxes. Mesoscale approaches thus provide the possibility of identifying behaviour in the coupled system against which large-scale models can be compared. There have been a variety of mesoscale observational and modelling studies focussing on the region. The sensitivity of event precipitation to land cover has been assessed with mesoscale simulations by Mohr *et al.* (2003) and Sogalla *et al.* (2006). Alonge *et al.* (2007) explored the impact of initial soil moisture on simulations of convection over a full diurnal cycle under typical Sahelian conditions. That study found significant increases in planetary boundary layer (PBL) equivalent potential temperature (θ_e) over wet soil compared to dry. The impact on θ_e of enhanced latent heat from the wet surface more than offset the effect of reduced sensible heat, an impact which was reinforced by weaker entrainment of low θ_e air from above the PBL. Though simulated precipitation developed slightly later over wet soil, the resulting convective lines were more intense and longer-lived than over the dry soil.

Using *in situ* data, Taylor *et al.* (1997) identified an unexpected persistence in rainfall gradients from one storm to another, accompanied by persistent anomalies in θ_e. Subsequent analysis of two years of data from a dense rain gauge network (Taylor and Lebel, 1998) confirmed the persistence of rainfall patterns. They compared rainfall from passing Mesoscale Convective Systems (MCSs) between pairs of neighbouring gauges ($\sim$10 km apart), finding that there was a strong preference for enhanced rainfall at stations which were already wet from storms in the previous two or three days. Using a cloud-resolving model of a squall line, this positive feedback mechanism was further investigated by Clark *et al.* (2003, 2004). They demonstrated a dominant impact of horizontal moisture gradients in the PBL on the dynamics of individual convective cells which could result in rainfall patterns persisting from storm to storm, especially on spatial scales of around 10 km.

More recently, Taylor and Ellis (2006) (hereafter TE06) used satellite data to identify a mesoscale soil moisture–rainfall feedback of the opposite sign (i.e. negative) in the Sahel. They used passive microwave data to map wet and dry soils over the course of a wet season, and analysed subsequent spatial patterns in cloud-top temperature to assess where deep convection was more favoured, over wet or dry areas. This study showed a strong suppression of convection over wet soils during the afternoon and early evening, when storms tend to initiate in response to daytime heating. The reasons for this behaviour could not be identified from the satellite data, though TE06 suggested two plausible alternative mechanisms for a negative feedback in the case of initiating convection, based on land–atmosphere studies elsewhere in the world.

The first mechanism considers the vertical profile of the atmosphere and its sensitivity to changes in soil moisture. Several authors have shown, using simple models of PBL growth, that whether moist convection develops preferentially over wet or dry soils depends on the initial profile. Ek and Holtslag (2004) used conditions for a single day in the Netherlands to illustrate that the sensitivity of the relative humidity at the top of the PBL to soil moisture depends on whether the effect of enhanced surface evaporation moistening the PBL is offset by that of weakened PBL growth. This balance is rather sensitive to the stability of the layer into which the PBL is growing. In a similar vein, Findell and Eltahir (2003) used soundings from across the United States to identify regions where enhanced soil moisture was likely to produce either enhanced or suppressed rainfall, or where surface fluxes would make little difference. Rabin *et al.* (1990) showed, using satellite observations and a one-dimensional model, that enhanced cloud cover was favoured over a warm surface, in this case due to land-use variations rather than soil moisture.

The second mechanism concerns the impact of horizontal variations in surface fluxes on the generation of mesoscale circulations (e.g. Segal and Arritt, 1992). A number of idealised mesoscale modelling studies have demonstrated that under appropriate large-scale conditions, contrasting surface features organised on length scales of several tens of kilometres can induce mesoscale zones of moisture convergence, favouring the initiation of moist convection during the afternoon (Anthes, 1984; Chen and Avissar, 1994; Emori, 1998). In these cases, precipitation is favoured over the warmer surface, i.e. over the drier soil in the case of soil moisture forcing. Studies which have found observational evidence for this mechanism in different atmospheric and geographical contexts include Carleton *et al.* (2001), Negri *et al.* (2004) and Wang *et al.* (2009).

Land–atmosphere feedbacks formed one of the foci of the African Monsoon Multidisciplinary Analysis (AMMA: Redelsperger *et al.*, 2006). The AMMA Special Observing Period provided a unique opportunity to make measurements capturing the coupling between the land and atmosphere in a region where such feedbacks are considered to be strong. A particularly important aspect of the measurements in this respect was a series of aircraft flights in the Sahel during July and August 2006 which targeted mesoscale variations in soil moisture. The aim was to examine how the PBL responded to variability in soil moisture, as identified from satellite data. Data from these flights showed for the first time in West Africa that soil moisture patterns were sufficiently well organised and intense to induce mesoscale circulations (Taylor *et al.*, 2007b). Analysis of chemical data also showed how closely the PBL concentration of NO_x and ozone mapped onto soil moisture via emission of NO from wet soil (Stewart *et al.*, 2008).

This paper presents a case-study in which the aircraft was targeting mesoscale soil moisture features as a major MCS developed. The availability of both *in situ* and high resolution satellite data provides an opportunity to explore the likely processes which lead to the climatological relationships between soil moisture patterns and the diurnal cycle of convection found in TE06. The study provides a detailed evolution of the system in the

region of the flight using satellite cloud imagery. The relationship of the storm to pre-existing soil moisture patterns is determined using satellite data from the land surface, whilst the aircraft measurements provide a quantification of the impact of surface patterns on variability in the PBL.

The data used in this study are described in the next section, whilst the antecedent soil moisture conditions, the flight track and an overview of the storm are presented in section 3. Section 4 provides an analysis of the initiation of the system using satellite data. The aircraft measurements in the PBL are presented in section 5, followed by analysis of the storm once it reached a mature stage.

2. Data

2.1. Satellite data

A number of satellite datasets were used in this study to map both spatial variability in soil moisture and the development of convective cloud. The primary source of data used throughout the AMMA aircraft campaign to identify the presence of wet and dry surfaces was land-surface temperature (LST) derived from the Spinning Enhanced Visible and Infrared Imager (SEVIRI) instrument on board Meteosat Second Generation (MSG). The Land Satellite Applications Facility (LandSAF) produces an LST product every 15 minutes in near real time, and with a spatial resolution ~3 km in this study region. The LST is computed using a generalised split-window technique in which LST is calculated as a linear function of clear sky top-of-atmosphere brightness temperatures in SEVIRI channels 9 (10.8 μm) and 10 (12.0 μm) (Caselles *et al.*, 1997; Trigo *et al.*, 2008). An additional screening technique was subsequently applied to the LandSAF LST data to remove pixels contaminated by cloud. The principle of this screening, performed on each pixel individually, was to remove periods when there was significant temporal variability in either the LST or visible (MSG channel 1) data inconsistent with the slowly changing diurnal signal expected from clear sky conditions. Finally, a dust detection algorithm (Chaboureau *et al.*, 2007) using the difference in brightness temperature between channels 9 (10.8 μm) and 10 (12.0 μm) was applied. These additional screening methods were applied to daytime LST for the period 21 May–10 October. To map the location of wet and dry surface patches on any particular day using information from different times during the day, deviations in cloud-free LST for each slot were computed relative to the longer-term mean diurnal cycle for every pixel. The resulting slot anomalies in LST were averaged over the day (0700 to 1700 local time) to produce a daily mean LST anomaly (LSTA). This product is useful for highlighting spatial variability in transient controls on LST (notably soil moisture) and reduces the influence on LST of permanent or slowly-varying factors such as vegetation cover. In this study, the longer-term averaging period was chosen to be the pre-monsoon phase from 1 June to 10 July 2006.

Whilst the daily LSTA data can provide a fairly accurate map of the location of relatively wet and dry surfaces, quantitative information on soil moisture from LSTA is limited, as the surface temperature response to soil moisture depends on many properties of the soil and vegetation. Quantitative satellite estimates of soil moisture, derived from passive microwave data on-board the Aqua satellite (Owe *et al.*, 2008) and representative of the top 1 cm or so, were compared with the LSTA product. Gruhier *et al.* (2008) have shown that this dataset does capture the temporal variability of Sahelian soil moisture, if not its absolute values.

To monitor the development of convection in the atmosphere, use was made of TIR (thermal infrared) data from MSG (channel 9), available at the same spatial and temporal resolution as the LST data. A climatology of wet-season cold cloud based on Meteosat 7 data for the period 1998 to 2005 was also used. In addition, for part of the day under study, MSG provided high resolution (~1 km) visible (channel 12) data within the target area which was used to identify the early stages of convection.

2.2. Aircraft measurements

The British Aerospace BAe146 aircraft operated by the UK Facility for Airborne Atmospheric Measurements was deployed for a 6-week period in July and August 2006 around Niamey, Niger. One of the aims of this deployment was to sample the daytime development of the PBL across heterogeneous soil moisture features. The aircraft was equipped with instruments to measure temperature and three-dimensional wind at 32 Hz (http://www.faam.ac.uk/). In addition to calculating mean dynamic and thermodynamic variables from these sensors, an estimate of sensible heat flux at the level of the flight was computed based on the covariance of the temperature and the vertical velocity about 30-second running means (approximately 3 km along the flight track). A Heimann radiometer was used to identify variations in land-surface temperature directly beneath the aircraft and a nephelometer measured scattering by aerosol. Finally, an Airborne Vertical Atmospheric Profiling System comprising Vaisala RD93 dropsondes (see http://www.eol.ucar.edu/isf/facilities/dropsonde/gpsDropsonde.html) was deployed on the flight.

3. Overview of case-study storm

3.1. The storm over its life cycle

The storm under examination was initiated around 1300 UTC on 31 July 2006 in northeastern Mali (1°E, 16.5°N) and propagated southwestwards across the country, reaching the Bamako area (8°W, 13°N) by 0600 UTC on 1 August. The precipitation from the storm during this period is shown in Figure 1, as estimated from the EPSAT-SG (Estimation des Pluies par SATellite – Seconde Génération: Chopin *et al.*, 2004) precipitation product from AMMA-SAT (AMMA-Satellite component: http://ammasat.ipsl.polytechnique.fr). Meteosat TIR

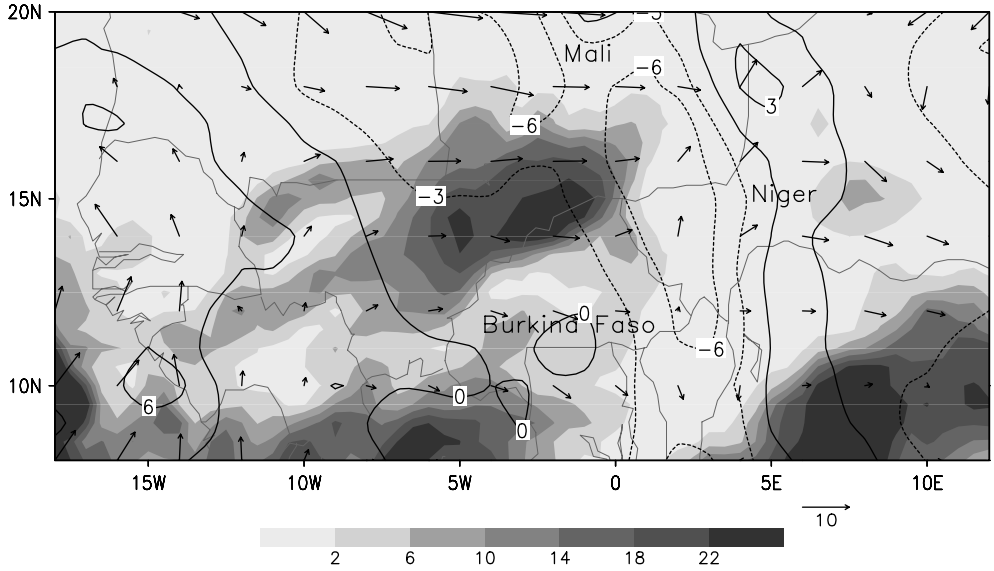

Figure 1. Twenty-four hour rainfall (shading; mm) to 1030 UTC 1 August 2006 from EPSAT-SG. Also shown are wind data from the 1200 UTC ECMWF operational analysis on 31 July (m s^{-1}); arrows indicate wind vectors at 925 hPa, contour lines denote meridional wind at 700 hPa.

imagery indicates that the system weakened around noon on 1 August, but redeveloped in early evening, and finally decayed off the West African coast on 2 August. The focus in this paper is the potential influence of the land surface (notably, antecedent soil moisture patterns) on the convection, both during its early afternoon initiation stage, and as it matured into a major MCS during the evening.

The synoptic environment in which the storm developed is also depicted in Figure 1 using data from the 1200 UTC European Centre for Medium-Range Weather Forecasts (ECMWF) operational analysis. At this time and longitude, the axis of the African Easterly Jet lay well to the south, around 11°N (not shown). The meridional wind at 700 hPa indicates that the storm developed in northerly flow at that level; a number of past studies have indicated that the northerly phase of synoptic systems in this region can have an increased likelihood of convective activity (e.g. Fink and Reiner, 2003). The boundary layer exhibited strong westerly flow (wind vectors shown at 925 hPa). The storm developed at the end of a two-week period of African Easterly Wave activity, three weeks after the onset of the West African monsoon in 2006 (Janicot *et al.*, 2008). This period was marked by a sequence of storms in northern Mali, during which time the vegetation began to develop (Taylor *et al.*, 2007a).

3.2. The aircraft track and antecedent soil moisture

The aim of the aircraft flight on this day was to sample the response of the PBL to mesoscale soil moisture heterogeneity induced by storms the previous day. Figure 2(a) shows the pattern of soil wetness prior to the flight using both LSTA and soil moisture derived from passive microwave data. Thermal infrared images from MSG indicate that storms developed around 1800 UTC on 30 July to produce wet patches P1 and P2 in the region around the town of Gao in Mali. During the evening, the southernmost storm (which created P1) intensified, with cloud-top temperatures reaching as low as −80°C. This created a third patch, P3, running west from the Greenwich meridian to around 2°W. A network of seven daily rain gauges across the AMMA mesoscale field site in the Gourma region to the west of Gao measured an average of 15 mm from this event, ranging from 0 to 30 mm at individual sites.

There is good qualitative agreement between regions with strongly negative LSTA and high values of soil moisture from passive microwave. Differences occur due to the contrasting spatial resolution of the instruments: ∼3 km for MSG and 30–60 km for the Advanced Microwave Scanning Radiometer (AMSR-E), depending on orientation (Richard De Jeu, personal communication). For example, patch P2 is not well-resolved by AMSR-E. The timing of the acquisition of the AMSR-E data relative to the storms also affects the retrieved soil moisture pattern. When the satellite passes over, at 0150 UTC on 31 July, the storm which creates P3 is still active, and accurate soil moisture retrieval is not possible beneath the storm (around 15°N, 1.5°W). Clearly, the satellite also cannot detect the western extremities of P3 as it has not yet rained there. The timing also likely overemphasises soil moisture in P3 (relative to P1 and P2) as the top centimetre of the soil will remain very wet for an hour or two after the storm.

The terrain of the region is predominantly flat, and at this stage of the season, generally had only isolated pockets of shrub and emerging herbaceous vegetation evident from the aircraft amidst predominantly bare soil. To the west of the river within P1 there were some more extensive patches of seasonally flooded woodland of up to 1 km in length. The dominant orographic feature (Figure 2(c)) is the Niger river valley, typically 70 m below the plain, which runs southeastwards past Gao. To the east and north of the river is higher ground, reaching 200 m above the plain in places.

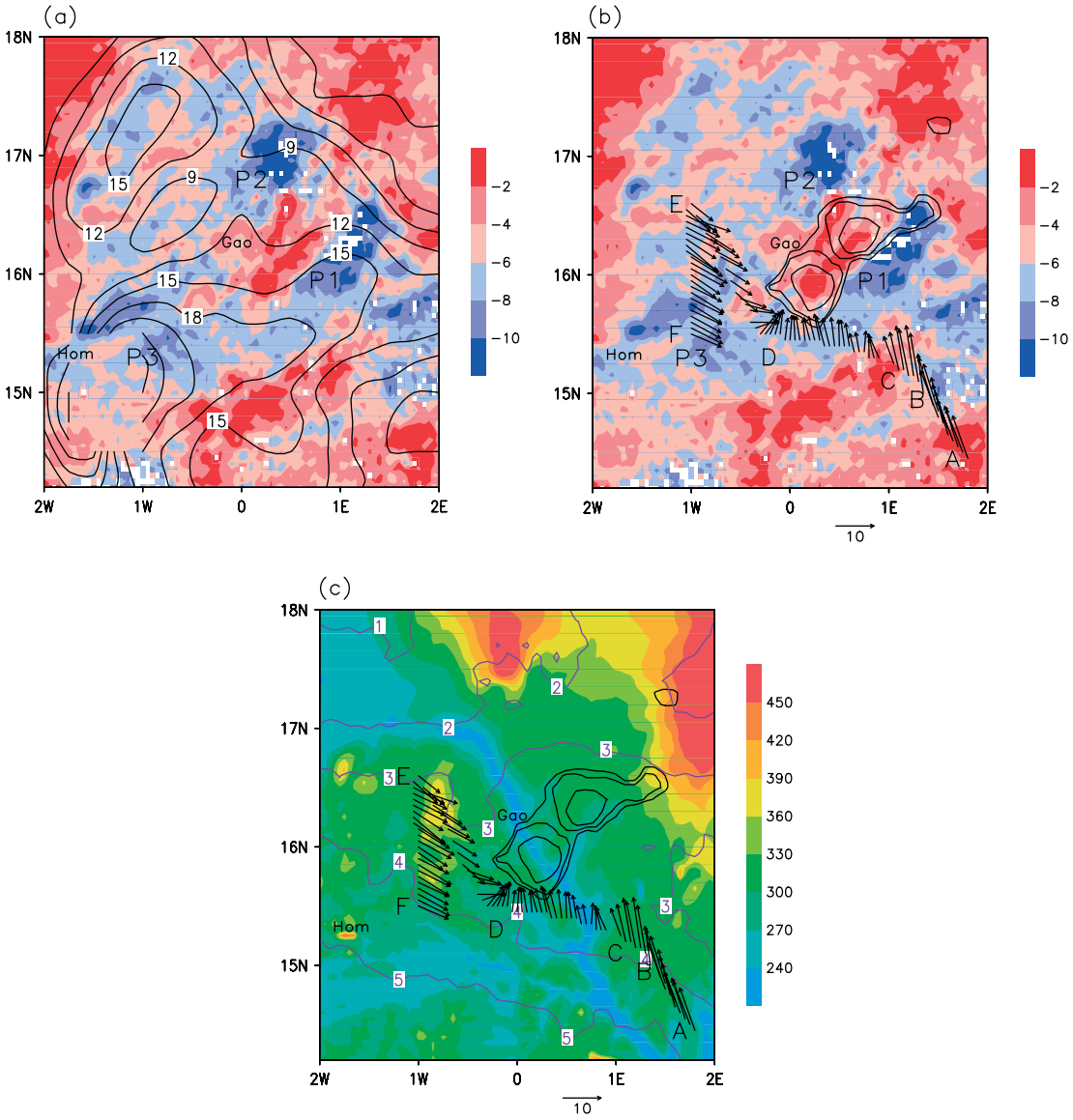

Figure 2. Land-surface temperature anomalies (°C; shading) gridded at a spatial resolution of 0.05 degrees on 31 July (a) and (b). White pixels denote missing data. The isolines in (a) depict volumetric soil moisture (%) from AMSR-E at 0150 UTC on that day. Note that active convection at that time prevents soil moisture retrieval in the southwest of the domain. Black contours at −50, −60, and −70°C in (b) and (c) depict the minimum TIR temperature from MSG during the early stages of the storm (1300 to 1530 UTC). In (c), the shading depicts the topographic height in the region (m) and the purple contours, the climatological occurrence of cold clouds (%; threshold of −40°C) during the afternoon period. The vectors in (b) and (c) denote the *in situ* winds measured by the aircraft along the flight track (m s^{-1}). The towns of Gao and Hombori, and points A to F along the track (see Table I) are marked, and wet patches P1, P2 and P3 shown in (a) and (b).

The initial plan for the aircraft flight was to perform an early afternoon PBL transect across patches P1 and P2. Take-off was delayed due to the passage of an MCS in the Niamey region during the morning of 31 July, and when the aircraft finally approached the target zone (point A in Figure 2 and Table I), radar echoes indicated the development of the storm directly on the flight path. This was unexpected as no storms had been predicted in the region by the AMMA forecast team. The location of the deep convection is indicated in Figure 2(b)–(c) from MSG TIR data. Visibility decreased over a period of minutes approaching B, forcing the aircraft to fly at higher altitude for safety reasons. A new course was plotted to go to the west of the storm and try to survey the upstream environment. The dust got progressively worse, before clearing dramatically as the aircraft emerged from the front of a haboob at C. The aircraft then returned to a height of 190 m above the ground to fly across the river valley to D, E and F ahead of the system. The aircraft then flew near the top of the PBL between E and F, before gaining altitude and launching a sequence of dropsondes ahead of the storm (on the transect between E and F) and behind it.

A potential trigger for convective initiation is topography. Figure 2(c) shows that the storm was initiated some 100 km to the southwest of a ridge reaching 200 m above the plain. Also shown in Figure 2(c) is an 8-year wet-season climatology of cold cloud constructed from Meteosat imagery between the hours of 1200 and 1700 UTC. This climatology indicates only a minor increase

Table I. Flight levels and timing of low-level legs on the flight.

Leg	level	Time (UTC)
A to B	170 m agl	1516–1525
B to C	600 m agl	1526–1532
C to D	190 m agl	1534–1552
D to E	190 m agl	1552–1612
E to F	190 m agl	1614–1630
F to E	950 m agl	1633–1649

agl = above ground level.

in afternoon convection downstream (southwest) of the ridge compared to the more zonal pattern elsewhere, as depicted by the northward excursion of the 3% contour in Figure 2(c). The lack of a strong climatological convection signal in the location where this storm actually developed suggests that topography was not the dominant factor in this case.

On the other hand, a striking aspect of the development of this storm was its location within the dry soil region between P1, P2 and P3 (Figure 2(b)). Such a location is entirely consistent with the analysis of TE06. They found a strong preference for convective initiation over dry soils within heterogeneous mesoscale soil moisture patterns, though the use of passive microwave data in that study precluded such a well-resolved view as depicted in Figure 2(b). In the next section, this apparent link between initiating convection and antecedent soil moisture is investigated in more detail, taking advantage of higher spatial resolution land-surface and cloud satellite data than were available in TE06.

4. Initiation of the storm

The early stages of the storm are well captured by both thermal and visible data from MSG (Figure 3). The grey scale shows visible radiation detected with the high resolution (1 km) sensor on MSG. This combines the effects of fixed land-surface features with the evolving cloud field and its shadows. A notable example of the former is a dark rocky region located over and to the east of P1. Developing convective cells are apparent as highly reflective, often fine-scale clouds, for example at 1315 UTC. These first appear in the region at 1200 UTC around 2°E, 16.4°N, and are still evident there 45 minutes later (Figure 3(a)). Figure 3(a) also depicts the first cells in the location where the storm later develops, oriented roughly along a southwest–northeast axis, coinciding with the northern edge of P1.

In the next 60 minutes, cloud develops rapidly along the northwestern edge of P1, and by 1345 UTC the temperatures at cloud top reach −40°C or less in places. The location of the clouds at this stage is strikingly similar to the pre-existing soil moisture gradient depicted by the LSTA contours, with cloud developing readily on the dry northwestern side. Elsewhere, cold clouds (less than −40°C) are found only to the southwest of the developing system. These are associated with less reflective, more homogeneous and long-lived structures, which may be cirrus. In later images (Figure 3(d), (e) and (f)), the convection expands westward across the dry area, organised into two distinct regions of low cloud temperatures. There is some deep convection apparent at 1445 and 1515 UTC over the northernmost part of P1, though this is short-lived. The convection apparent throughout the sequence some 100 km to the northeast of patch P1 finally deepens to reach a cloud-top temperature of −40°C by 1515 UTC. This system continues to grow and propagate westwards until it reaches P2 around 1830 UTC (not shown), where it decays. Finally, the dust front (marking an advancing cold pool) which affected visibility on the flight becomes clear in later images. For example, in Figure 3(f) a linear structure is apparent, propagating northwestwards away from the southeast corner of the image, with dusty, more reflective conditions behind it. The timing and location of this front is consistent with measurements on the aircraft (discussed in the next section).

The horizontal extent of the storm in its early stages appears to be linked to the presence of dry soil; there is only minor convective development over adjacent wet soil, consistent with TE06. What is evident in this case is that the storm triggered very close to, but on the dry side of, the northwestern edge of patch P1. The development of convection parallel to the edge of P1, and the lack of initiation on the opposite side of the dry area (i.e. on the southeastern edge of P2) provide important clues as to the mechanisms responsible for the observed suppression of convection over wet (relative to nearby dry) soil. According to the midday (i.e. pre-storm) ECMWF analysis, supported by surface observations and dropsonde winds, the flow in the PBL was from the westnorthwest. Initiation therefore occurred upstream of the wet soil, in terms of the large-scale flow. It is reasonable to assume that the soil moisture pattern induced surface heating gradients of a similar strength to those sampled the following day by the aircraft (Taylor *et al.*, 2007b). In that case, temperature and wind data showed convergence over dry soils and divergence over the wet. Idealised simulations (e.g. Segal *et al.*, 1988) show that surface-induced circulations are distorted by the large-scale flow such that convergence is enhanced at the downstream edge of a dry (warm) feature where the mesoscale flow opposes the background wind. In this case, that downstream edge corresponds to the northwestern side of P1, where convection first developed. Conversely at the upstream edge of the warm feature (the southeastern boundary of P2), convergence would be weakened by the action of the large-scale flow, which degrades the surface pressure gradient through advection from a cool to a warm PBL. Thus we might expect *a priori* that if a surface-forced circulation was important for the initiation of the storm, that storm would trigger in the observed location.

Unfortunately, the aircraft arrived in the region after the storm had begun to develop, and so there are no pre-storm measurements in the location of initiation. The *in situ* winds measured by the aircraft to the south and

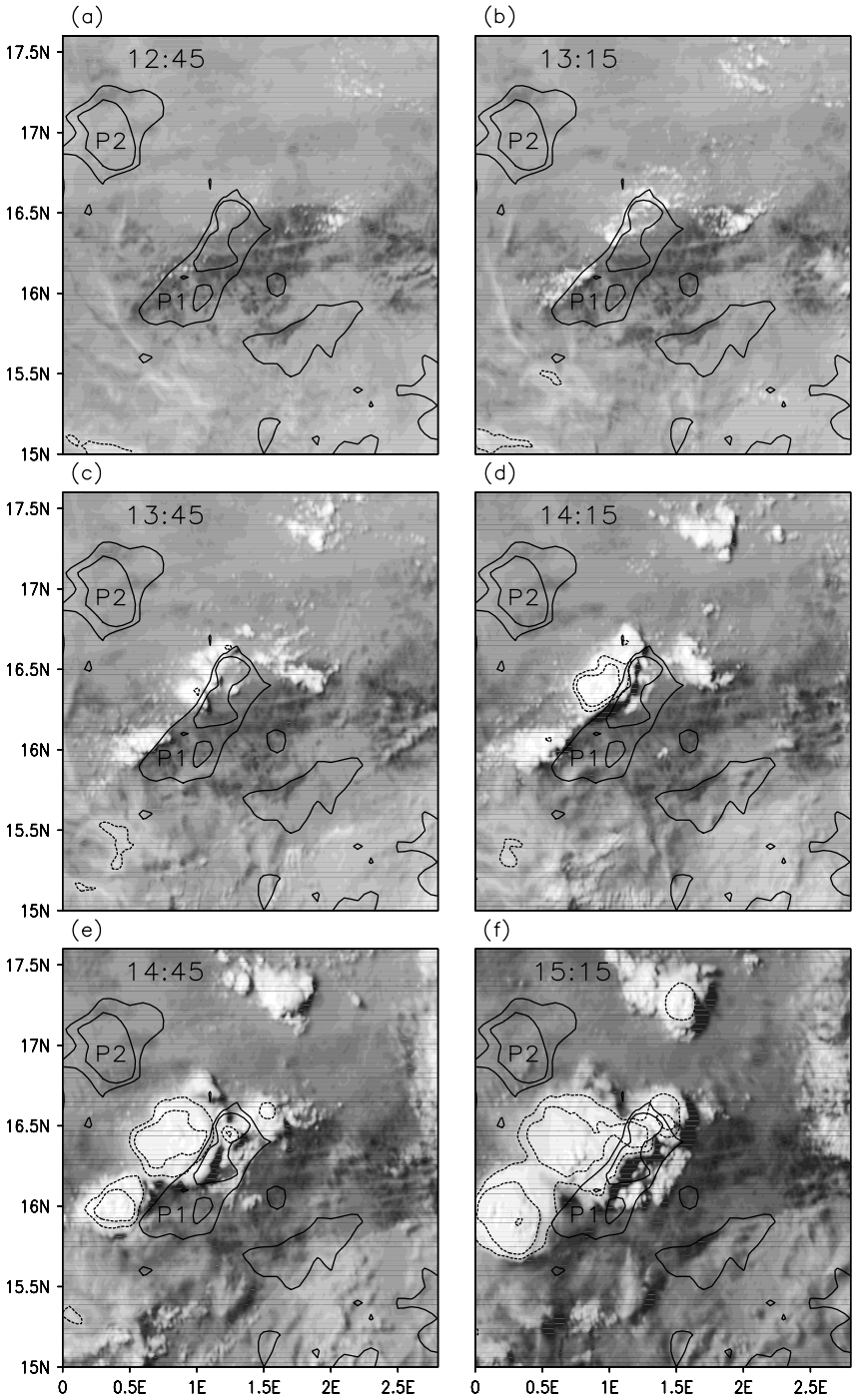

Figure 3. Visible imagery (shading) every 30 minutes between 1245 and 1515 UTC on 31 July. Solid contours show LSTA data gridded at 0.1 degree resolution at values of −10 and −8°C. Cold cloud tops from TIR data are shown with dashed lines at −40, −60 and −80°C.

west (Figure 2(b)–(c)) indicate strong convergence into the storm, with variations in the horizontal PBL wind speeds of up to 10 m s^{-1} as well as strong southerly winds associated with the density current close to B and C. Under these conditions, it is not possible to identify any pre-storm surface-induced mesoscale flows from the observations. Such surface-induced flows are expected to be weaker than the mesoscale flow drawn into the growing storm, as shown for example on the following day by Taylor *et al.* (2007b), where surface-induced wind anomalies of the order of 1–2 m s^{-1} were observed.

Examination of satellite cloud imagery at the larger scale reveals that the initiation of the storm was coincident with the arrival of a linear cloud band. This propagating feature is distinct from the cold pool (evident from the dust front in Figure 3) which arrived several hours later. Figure 4 shows the cloud band, identified as a line of intermittent cold pixels, propagating westward and northwestward from the large well-established MCS tracking across Burkina Faso. At 1200 UTC, this band can be seen extending from 2°E, 15.5°N down to 2°W, 13°N, and thereafter arcing round to the southeast. The

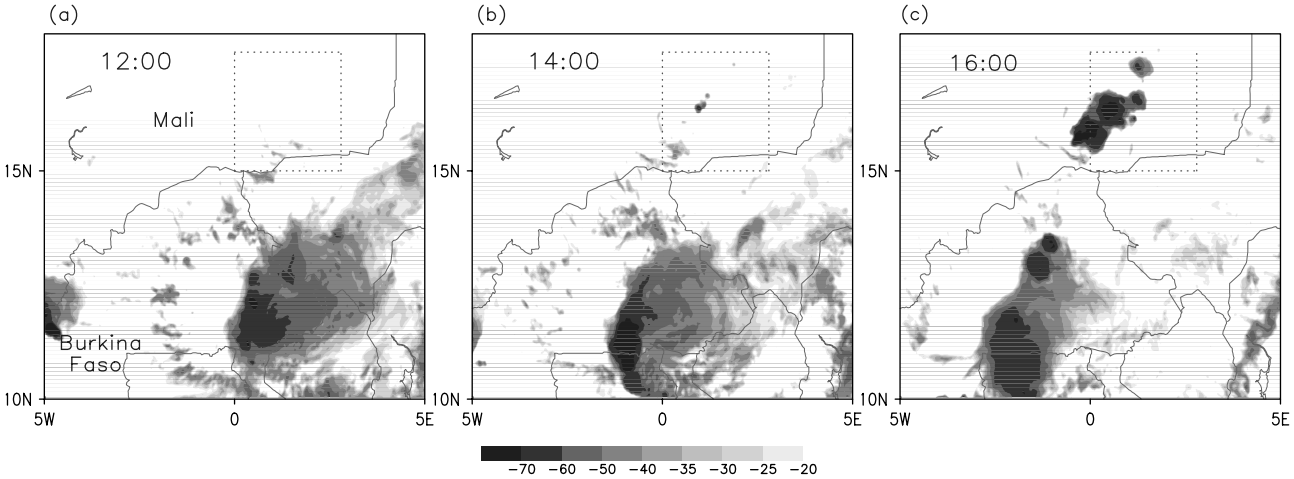

Figure 4. Brightness temperature images (°C) depicting cold cloud at (a) 1200, (b) 1400 and (c) 1600 UTC. The domain in Figure 3 is marked by the dotted lines.

cloud feature at this time was about 250 km ahead (west) and to the north of the mature MCS. The progress of the leading edge of the cloud band has been hand-drawn in Figure 5. The nature of the clouds on this band is not clear to us, though they are apparent both in visible and TIR fields as northwest to southeast-oriented ribbons, around 50–100 km long, 20 km wide, and with brightness temperatures of around −10 to −40°C. Behind the line of the cloud band, the cloud elements disappear. Only at the study area, characterized by strong soil moisture contrasts, was a major convective system triggered.

The propagating cloud band was running around 100 km ahead of, and somewhat faster than the cold pool which had been generated by the southern storm. The cold pool (clearly apparent in the southeast of Figure 3(e)–(f)) has also been sketched in Figure 5. Around the time of the initiation of the first cells (between 1230 and 1300 UTC in visible imagery), the leading edge of the cloud band was passing over the initiation region, while the gust front was still some 150 km to the southeast. Overall, the propagation speed of the gust front was around 7.6 m s^{-1}, while that of the cloud band was around 13 m s^{-1} (estimated from a distance–time plot of TIR, aligned along the direction of propagation; not shown). The nature of the cloud band and its possible relationship to the cold pool are not easy to establish from the data available here, but some possibilities are discussed in section 7.

5. Spatial variability in the PBL from the aircraft

In this section, data from the aircraft are analysed and interpreted in terms of variability in the underlying surface. Figure 6 presents measurements taken as the aircraft flew from points B to F, to the south and west of the developing storm (Figure 2). The emergence of the aircraft from the dust front at 1532 UTC is indicated by the sharp drop in scattering recorded by the nephelometer in Figure 6(b). This also shows the presence of increased atmospheric dust loading from point D onwards.

The LSTA data from along the track (Figure 6(a)) provide an indication of where recent rainfall has occurred. The most pronounced cool (i.e. wet) surface feature, in terms of both amplitude and extent, was encountered shortly after point C, corresponding to a transect across the southern part of P1 towards point D. This section, a distance of approximately 120 km on the flight track, is highlighted in grey throughout Figure 6 and was predominantly cloud-free during the flight. The area around C itself was dry according to LSTA data. After crossing P1, the aircraft flew northwestwards (to E) and then due south (to F). During this period of the mission the aircraft overflew notable dry features shortly after D (1554 to 1559 UTC) and around E (1611 to 1616 UTC) in otherwise relatively wet conditions, according to the LSTA data.

The onboard downward-looking radiometer recorded surface temperatures which agreed in many respects with the LSTA sequence. In particular, the crossing of P1 was marked by a decrease in surface temperature of the order of 10°C relative to the drier zones either side. However, some smaller-scale features detected by LSTA (relative to pre-monsoon temperatures) are not evident in the on-board data. This may be explained by several factors. Transient influences on surface temperature via radiation (i.e. dust and cloud) are removed from the LSTA data, but may be important for the instantaneous data recorded by the onboard radiometer. It should also be noted that between B and C, the surface temperature signal is likely to have been affected by both the presence of the dust beneath the aircraft, and the increased altitude of the platform. In addition, LSTA captures differences in surface temperature relative to dry, pre-monsoon conditions, in order to reduce the influence of permanent surface features such as sand dunes. On the other hand, the absolute surface temperature patterns on this day will be affected by such fixed landscape factors.

An estimate of sensible heat flux recorded by the aircraft is presented in Figure 6(b), and indicates a strong suppression of this quantity when crossing P1. Elsewhere,

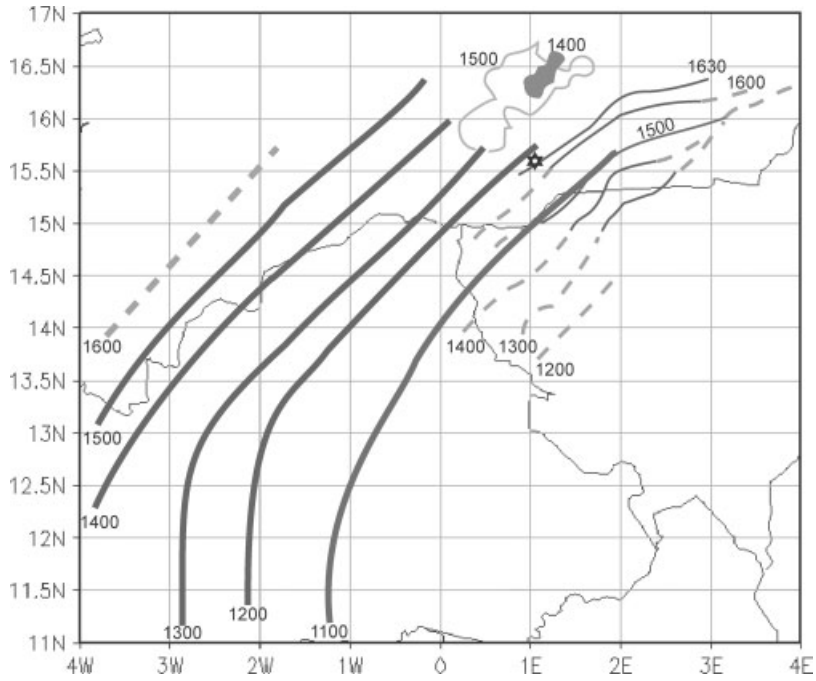

Figure 5. Position of the leading edge of the mid-level cloud band (thick lines) and the low-level gravity current (thin lines), as derived from individual plots of TIR and VIS MSG data, respectively. Times for each line are indicated (UTC) and locations where the features are indistinct in the imagery are dashed. The closed contours indicate the times and sizes of the target storm, at 1400 (filled contour) and 1500 UTC. Where it was apparent in the VIS imagery, there was no significant cold cloud at the gravity current front. However, the gravity current front was contiguous with the leading edge of the cold cloud associated with the parent storm in the south, supporting the idea that it was a coherent part of the cold pool of the parent storm.

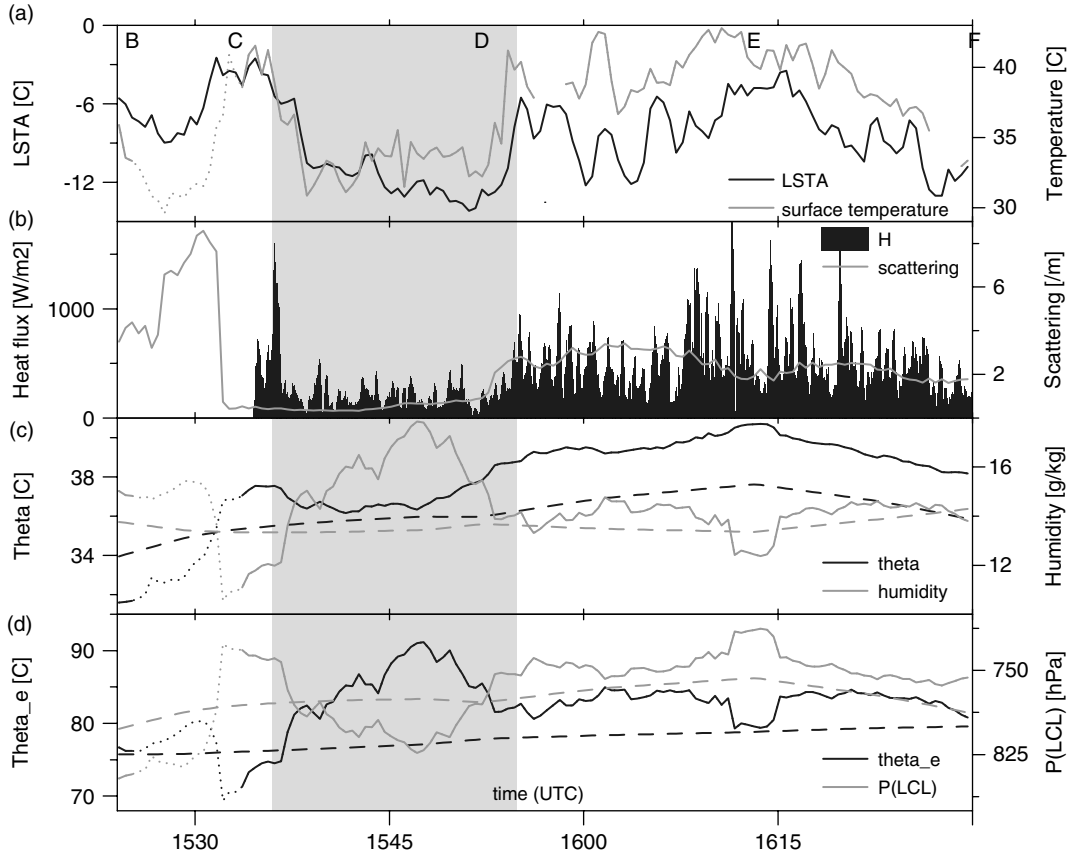

Figure 6. Time series of data from low-level run. (a) LSTA and surface temperature from the onboard radiometer (°C). (b) Aerosol scattering (m^{-1}) and turbulent heat flux (H; W m^{-2}). (c) Potential temperature (°C) and humidity mixing ratio (g kg^{-1}). (d) Equivalent potential temperature (°C) and pressure at the lifting condensation level (hPa). Dotted lines denote data measured by aircraft above 300 m and dashed lines in (c) and (d) indicate variables in the ECMWF midday analysis at 925 hPa. The grey shading illustrates the passage across patch P1.

turbulent heat flux tends to be stronger in the 7 minutes after passing point D, and in the period around point E. In both cases, LSTA data suggest relatively dry surface conditions.

In Figure 6(c), *in situ* measurements of potential temperature and humidity mixing ratio are presented to highlight along-track mesoscale variability in these properties. Additionally, to illustrate the effect of the aircraft flying in a region of significant large-scale gradients, data from the ECMWF midday operational analysis are shown. Analysed potential temperature and humidity mixing ratio at 925 hPa have been interpolated horizontally onto the flight track from a 1 degree grid. The large-scale patterns from ECMWF data suggest temperatures 3°C higher in the north (point E) compared to point B in the south, accompanied by a modest drying of less than 1 g kg^{-1} between these locations. The observations show that superimposed on these features, the PBL temperature falls by up to 2°C above P1 relative to the drier adjacent surfaces, with moistening by up to 4 g kg^{-1}. This variability is qualitatively consistent with high evaporation and low sensible heat flux from a wet surface. Other weaker mesoscale features are found after point D (1554 to 1601 UTC) and around point E (1611 to 1615 UTC). These are both warmer and drier than adjacent areas and marked by local maxima in LSTA, indicative of drier soil. Other local maxima in LSTA (around 1606 and 1623 UTC) produce no readily discernible influence on the PBL properties. Finally, the emergence of the aircraft from the cold pool at C is marked by very sharp transitions in temperature and humidity.

The contrast between the PBL above P1 and the adjacent drier surfaces corresponds to an increase in equivalent potential temperature of up to 15°C and increase in pressure at the lifting condensation level of nearly 100 hPa (Figure 6(d)). Such strong horizontal variations in thermodynamic properties are likely to influence the likelihood and intensity of deep convection under suitable atmospheric conditions.

The dropsondes launched ahead of the storm provide an indication of the vertical structure of the lower atmosphere and its sensitivity to soil moisture. Two of these profiles, close to points E and F, are shown in Figure 7; each of these profiles is typical of this climatic zone, with a well-mixed convective boundary layer growing into a near-neutral Saharan Air Layer (SAL), extending up to around 570 hPa (see Parker *et al.*, 2005). The land surface around point F (Figure 7(a)) was predominantly wet whilst point E (Figure 7(b)) coincided with locally dry soil, though neither location was optimal for capturing the extreme conditions sampled earlier on the flight between C and D. The profile above wet soil (Figure 7(a)) shows a well mixed PBL extending up to 850 hPa with values of temperature and humidity consistent with values recorded on the low-level transect close to that location. Over the drier surface (Figure 7(b)), the inversion is only slightly higher (800 hPa), though the PBL is 2°C warmer, and 2.5 g kg^{-1} drier. These differences in PBL properties are in part linked to their locations on the large-scale meridional gradients characteristic of the Sahel. However,

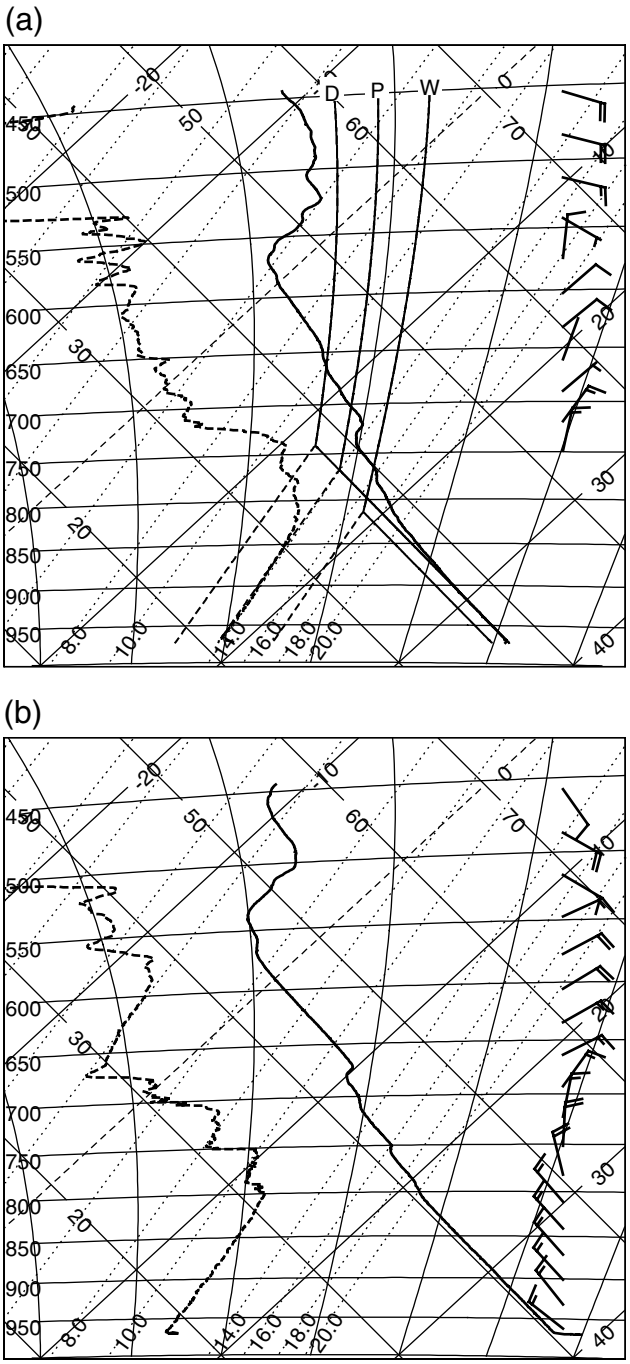

Figure 7. Tephigrams from dropsondes launched at (a) 1725 UTC, 1.1°W, 15.5°N (point F in Figure 2) and (b) 1711 UTC, 1.0°W, 16.6°N (point E in Figure 2). Also shown in (a) are parcel ascents assuming low-level conditions as observed (marked P), and using alternative low-level temperature and humidity measured above dry (D) and wet (W) soils.

as the sharp transition in θ_e to the south of E indicates in Figure 6, they also reflect the contrast in surface sensible and latent heat fluxes driven by soil moisture from storms the previous evening.

To provide an assessment of how soil moisture may have affected the thermodynamic profiles without the complication of the large-scale gradients in temperature and humidity, parcel ascents have been plotted on Figure 7(a) based on conditions sampled at approximately

the same latitude on the earlier transect between C and D. Parcels from both the extreme wet and dry air are used. There is a strong contrast in the level of free convection (LFC) in these two parcel ascents: 770 hPa for the wet parcel and 660 hPa for the dry. One cannot compute accurate values of Convective Inhibition (CIN) from the parcel ascents, as surface heating will have a significant impact on the temperature profile beneath 800 hPa due to entrainment. However, it seems likely that values of CIN above the dry soil would be, if anything, larger than over the wet soil. That being so, there would be no advantage for earlier convection over a dry soil as compared to a wet one as it would be associated with both a substantially higher LFC and no reduction in CIN. This implies that the one-dimensional thermodynamic profile arguments for preferential initiation over dry soil do not apply in this case. Thus the localised nature of convection over (and on the boundary of) dry soil in the early stages of the storm appears to be linked to the presence of surface-forced convergence, enhanced by the arrival of the gravity wave and cloud band from the southeast.

Once initiated, the energy available to the developing storm is related to the buoyancy of parcels in the updraught, whose integral is estimated by the convective available potential energy (CAPE). We cannot accurately compute CAPE in this case, as the dropsondes were released from the mid-troposphere and there are no profile data available above this level. However, we can compute the temperatures of the ascending parcels and use these to estimate the difference in CAPE between the two ascents, corresponding to the area on the tephigram lying between the pseudoadiabats followed by each parcel (see Parker, 2002). Here we compute the CAPE difference between 715 hPa, which represents an average of the two parcels' levels of free convection, and 150 hPa, which is approximately the tropopause in the 1200 UTC Niamey radiosonde ascent. In this way, we can infer that CAPE for the moist parcel will exceed that of the dry parcel by more than 3300 J kg^{-1}; a substantial amount (pseudoadiabatic ascent assumed). The next section describes observations of the mature convective system and its relationship to the surface.

6. Evolution of the mature storm

Figure 8 presents TIR data to depict the evolution of the storm relative to the underlying soil moisture features as it developed into an MCS during the evening. At 1630 UTC, the most active convection is occurring over the dry zone near point D. There is still little in the way of cold cloud over the wet patches. An hour later however, the storm has intensified as it starts to cross P3. In addition, distinct new areas of activity have developed over dry soils in a line towards the southwest. These are approximately aligned with the leading edge of a further extensive area of convection south of 13.5°N. At 1830 UTC, much of P3 is covered by cold cloud, reaching −85°C in places. This phase of the storm sees the maximum extent of cloud colder than −70°C. By 1930 UTC, the westward advance of this deep convection has slowed markedly compared for example to the −60°C isotherm, and the coldest cloud remains over P3.

Cold cloud tops are not well related to surface precipitation at this scale, but information on the location of rainfall can be gained from an overpass of TRMM (Tropical Rainfall Measurement Mission satellite) at 1935 UTC. Following Mohr and Zipser (1996), isolines of 85 GHz polarisation-corrected temperature suggest that heavy rain is occurring across the area around P3, but has not advanced into the drier zone ahead at this stage of the storm. Subsequent TIR images (not shown) depict a delayed advance of cold cloud tops across the drier soils to the west, before the storm finally reinvigorates around 2130 UTC, 150 km to the west of its location in Figure 8(d).

This sequence provides some evidence to support the hypothesis that once the MCS has reached a mature phase, with a quasi-linear leading edge (Figure 8(b)), the deepest convection occurs in areas where the soil was previously wet, consistent with e.g. Alonge *et al.* (2007) and Clark *et al.* (2003). Figure 9 presents data from the north–south transects between E and F to investigate this point in more detail. *In situ* measurements from the aircraft indicate a sharp drop in θ_e north of 16.4°N, approximately coincident with the northern edge of P3. The dropsonde data released ahead of the storm support this finding. Figure 9(c) shows that the first location along the transect to be affected by the storm advancing from the east is between 15.5 and 16°N. At 1715 UTC a newly developed area of convection arrives some 100 km to the south over a dry surface. Given the propagating nature of these storms, the development of convection along the transect is clearly sensitive to upstream convection. However, what is interesting here is the similar location of the sharp fall in θ_e north of 16.4°N, and the northward extent of the cold cloud. The cloud-top temperature never reaches −70°C north of this transition.

7. Discussion

In the case studied here, there appear to be several key mesoscale ingredients in the development of this major storm: a convergence zone produced by dry soil surrounded by wetter areas, the arrival of a gravity wave and, once the storm had become organised, the presence of wet soil downstream. In the case of initiating convection, the analysis of TE06 showed a clear signal, favouring new storms over dry soils rather than wet. In this region of intermittent convection, storm initiation is more likely controlled by inhibition than convective available potential energy. In the current study, all the areas of new convection occurred over dry soil, and appeared to develop in association with a gravity wave linked to an existing MCS. The most active growth of convection occurred on a strong soil moisture gradient where surface-induced low-level convergence was likely maximised. The gravity wave may also have contributed to the development of the storm some 100 km to the northeast; this

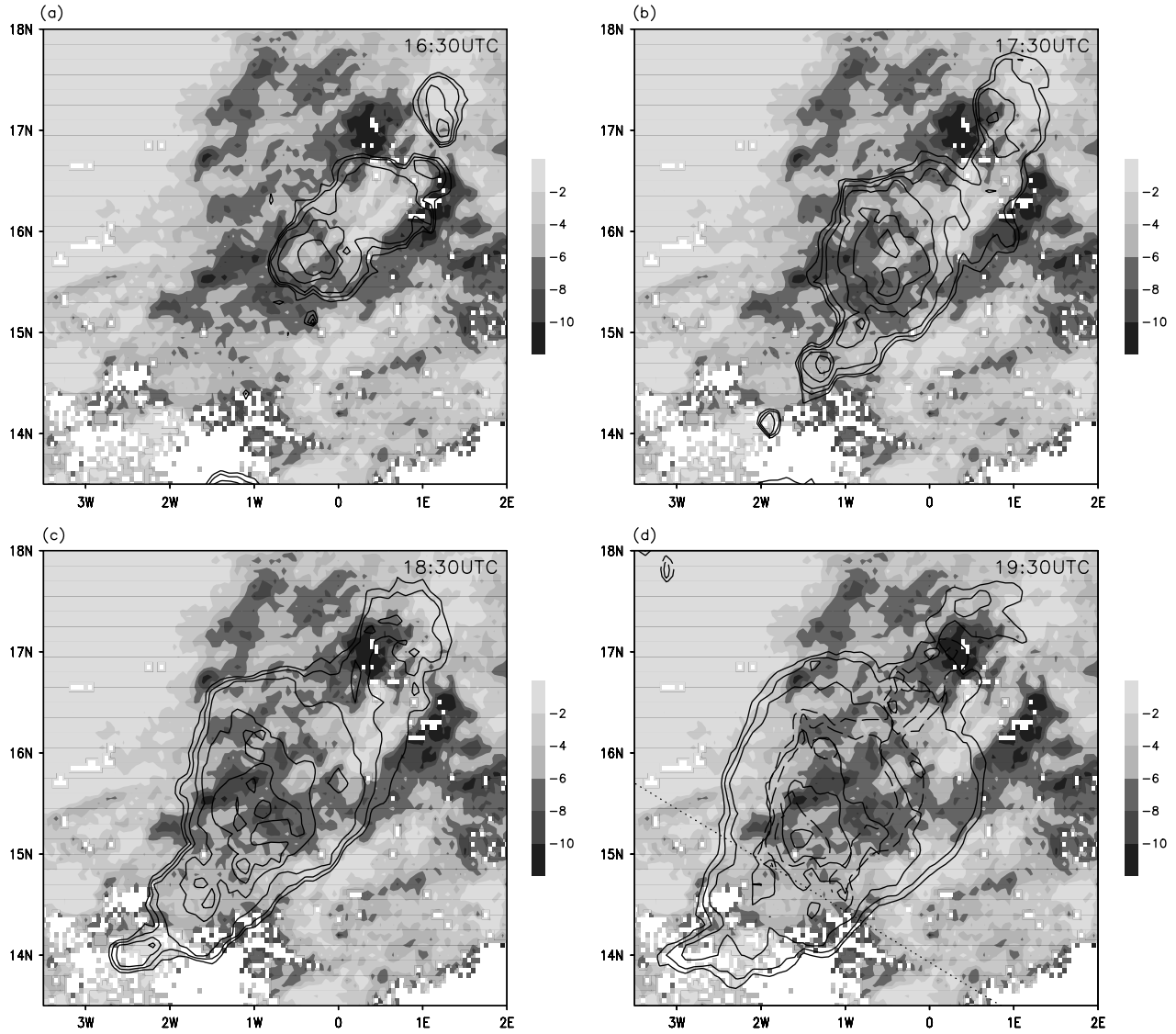

Figure 8. Hourly sequence of cold cloud brightness temperatures (contours at −40, −50, −60, −70, −75, −80°C) between 1630 and 1930 UTC 31 July relative to LSTA (shading; °C). In (d), the dashed lines show the 85 GHz polarisation-corrected temperature from TRMM at 150, 225 and 250 K, and the dotted line denotes the southwestern edge of the TRMM swath. White pixels denote missing LSTA data.

second, weaker, growth took place well away from wet soil, on the western slope of a ridge 200 m above the plain (Figure 2; 17.2°N, 1.5°E). The other areas of new convection in the region occurred around 1730 UTC (Figure 8), linked with the organised line of convection which had by then developed to the northeast. The new convection, which rapidly merged with the larger storm to the north, developed on dry soils adjacent to a wet surface feature ∼100 km across, centred at 14°N, 1°W.

In terms of the preferential initiation of convection over dry soils in the Sahel, further analysis of high resolution satellite data over multiple events is needed to extend the coarse resolution analysis of TE06. This should help to establish the relative importance of gradients in soil moisture versus uniform dry soils, and place the results in the context of other better understood controls on initiation, notably orography and cold pools.

A plausible explanation for the behaviour of the mature storm described in section 6 is that convection within the MCS was sustained by the higher moisture mixing ratios in the PBL overlying the wet surface. This explanation is entirely consistent with previous cloud-resolving model simulations (Clark *et al.*, 2003; Alonge *et al.*, 2007). Within a mature MCS, the downdraught running ahead of the system forces ascent and can raise PBL air to the LFC. At this point, there is a strong energetic advantage for cells developing above a wet soil. Clark *et al.* (2003) showed how this could trigger an additional cloud dynamical response, leading not only to enhanced convection within the cell feeding off moist air, but a suppression of neighbouring cells. In that model, pre-storm PBL gradients in θ_e could produce rather strong gradients in rainfall, a signal which emerges clearly when averaging over many convective cells. The northward extent of cold cloud in the case studied here may well have been linked to such a process, consistent with the modelling studies discussed above. Numerical modelling experiments of the storm are planned which will better

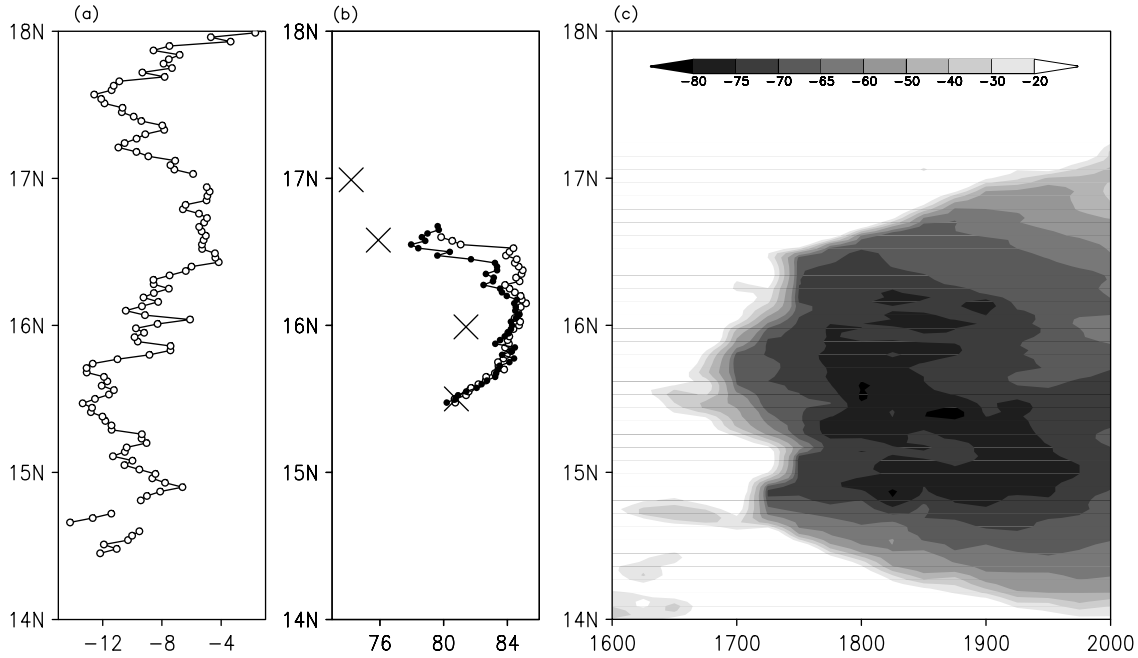

Figure 9. Data on a meridional transect at 1°W. (a) LSTA (°C), (b) Equivalent potential temperature (°C) from *in situ* data 190 m (open circles) and 950 m (closed circles) above the ground, and (crosses) from four dropsondes launched by the aircraft. (c) Evolution of cold cloud brightness temperature on the transect (°C).

isolate the role of soil moisture. Ongoing analysis of satellite data over multiple events will also better establish the relative importance of soil moisture gradients on mature MCSs.

We now consider the nature of the propagating cloud band which appears to have been critical in determining the timing of the first convection. The cloud band is consistent with the passage of an atmospheric wave feature; either a solitary wave (or bore), or a wave-front in response to the strong forcing of the storm to the south (e.g. Bretherton and Smolarkiewicz, 1989; Parker and Burton, 2002). Either of these phenomena remains possible in this case.

A number of previous authors have described observations and modelling studies of bores propagating ahead of a convectively generated gravity current (in this case the convective cold pool coming from the southeast), e.g. Koch *et al.*, 2008. Typically, such events consist of a bore propagating on a stable nocturnal inversion, and occur when the gravity current speed is lower than that of small-amplitude waves on the low-level inversion (Haase and Smith, 1989). In the case discussed here, the thermodynamic profile is rather different to the nocturnal cases, having a well-mixed boundary layer in the late afternoon capped by a near-neutral SAL (Figure 7(b)). However, this profile, with a stable layer lying between two near-neutral layers, also shows potential to support a solitary wave. If the wave is indeed this kind of bore-like structure riding on the interface between the monsoon layer and the SAL, then the implications for convective triggering in the northern Sahel are significant. The dropsonde profiles of Figure 7(a) show that for the range of parcels considered, the level of free convection is within the SAL – therefore within the potential lifting offered by a solitary wave. The neutrality of the SAL also means that a parcel displacement upward from the convective mixed layer requires much less energy than would be needed in the case of a stratified free troposphere (equivalently, the neutrality of the SAL leads to a relatively low CIN). A disturbance of given energy leads to a relatively large vertical displacement into the SAL.

One piece of evidence which somewhat opposes the idea of the gravity wave being a solitary wave on the CBL/SAL interface is that the cloud ribbons observed on the cloud band itself are at a much higher altitude, with temperatures of -10 to -40°C. We do not know at what altitude the air in these clouds originated, but their lack of reflectivity in the visible suggests cirrus. If the cloud ribbons represent high-altitude lifting of the air, then the wave feature is probably not confined to low levels (as a bore would be) but represents a wave-front emanating from the early stages of initiation of the parent MCS in the south.

Unfortunately we lack suitable surface observations of this case to describe the structure of the propagating wave in any detail. Whatever the true nature of this mesoscale wave, right now we can state that the initiation of the storm coincided with the arrival of a wave-front which extended over several hundred kilometres and emanated from the southern storm. At no other point on the wave-front was a long-lived storm produced.

8. Conclusions

This paper provides a detailed case-study of the impact of soil moisture patterns on the evolution of a subsequent major storm in the Sahel. A unique set of observations combining satellite and aircraft measurements provide

insight into the feedback mechanisms responsible. Data from the aircraft show a strong link between properties of the PBL and the underlying soil moisture, as inferred from satellite land-surface temperature imagery. Increases of up to 4 g kg^{-1} in PBL humidity mixing ratio were detected over wet soils relative to nearby drier zones, accompanied by decreases in temperature of 1 to 2 K. These contrasts lead to mesoscale differences in θ_e of 10–15 K and differences in the estimated level of free convection of over 100 hPa.

Directly ahead of the aircraft on the planned track, a storm was initiated during the early afternoon. The location of the cloud bore a striking resemblance to pre-existing soil moisture features; the first clouds appeared along a gradient in soil moisture produced by a storm the previous evening. The convection rapidly deepened and expanded to cover a region of dry soil, surrounded by wetter surface conditions. The location of the initiating convection occurred in the most likely location for strong soil moisture-induced convergence. This suggests that mesoscale land heterogeneity may play an important role in the initiation of storms remote from better understood zones of preferential convective initiation, such as orography. The arrival of a gravity wave from a remote MCS coincided exactly with the timing of the storm initiation, and therefore seems to have stimulated the initiation of the storm. Elsewhere in the region the propagating gravity wave did not produce any storms, confirming the significance of the soil moisture patterns in causing this event.

By late afternoon, the storm developed into a westward-propagating MCS. Satellite imagery indicates that the most intense convection associated with the storm occurred over pre-existing wet soils. The weakening of the convection away from the wet surface is consistent with a strong reduction in θ_e, as detected by the aircraft.

This case-study has demonstrated the validity of using land-surface temperature data from satellite to qualitatively infer PBL gradients in thermodynamic properties. Analysis of many cases using these satellite data are needed to extend the results presented here, in order to generate more robust statistics of the relationships between soil moisture and convection. This will help to clarify the key mechanisms influencing convection at the mesoscale, and assess their representation in atmospheric models.

Acknowledgements

We would like to warmly thank all those involved in the Niger deployment of the FAAM aircraft, and in particular Captain Al Roberts and Adrian Matthews for their contributions in the air during this somewhat unconventional flight. Based on a French initiative, AMMA was built by an international scientific group and is currently funded by a large number of agencies, especially from France, the UK, the US and Africa. The authors were funded jointly by the European Community's Sixth Framework Research Programme and the UK NERC project NE/B505597/1. We would also like to thank Land-SAF for the provision of land-surface temperature data, and EUMETSAT for cloud data, Matt Garvert for model simulations, Doug Clark and two anonymous reviewers for their useful comments, and James Groves (NCAS) for assistance with graphics.

References

Alonge CJ, Mohr KI, Tao W-K. 2007. Numerical studies of wet versus dry soil regimes in the West African Sahel. *J. Hydrometeorol.* **8**: 102–116.

Anthes RA. 1984. Enhancement of convective precipitation by mesoscale variations in vegetative covering in semiarid regions. *J. Clim. Appl. Meteorol.* **23**: 541–554.

Bretherton CS, Smolarkiewicz PK. 1989. Gravity waves, compensating subsidence and detrainment around cumulus clouds. *J. Atmos. Sci.* **46**: 740–759.

Carleton AM, Adegoke J, Allard J, Arnold DL, Travis DJ. 2001. Summer season land cover – Convective cloud associations for the Midwest US 'Corn Belt'. *Geophys. Res. Lett.* **28**: 1679–1682.

Caselles V, Valor E, Coll C, Rubio E. 1997. Thermal band selection for the PRISM instrument.1: Analysis of emissivity-temperature separation algorithms. *J. Geophys. Res.* **102**: 11145–11164.

Chaboureau J-P, Tulet P, Mari C. 2007. Diurnal cycle of dust and cirrus over West Africa as seen from Meteosat Second Generation satellite and a regional forecast model. *Geophys. Res. Lett.* **34**: L02822, DOI:10.1029/2006GL027771

Charney JG. 1975. Dynamics of deserts and drought in the Sahel. *Q. J. R. Meteorol. Soc.* **101**: 193–202.

Chen F, Avissar R. 1994. Impact of land-surface moisture variability on local shallow convective cumulus and precipitation in large-scale models. *J. Appl. Meteorol.* **33**: 1382–1401.

Chopin F, Bergès JC, Desbois M, Jobard I, Lebel T. 2004. 'Multi-scale precipitation retrieval and validation in African monsoon systems.' Paper presented at 2nd International TRMM Science Conference, 6–10 September 2004, Nara, Japan.

Clark DB, Xue Y, Harding RJ, Valdes PJ. 2001. Modeling the impact of land surface degradation on the climate of tropical north Africa. *J. Climate* **14**: 1809–1822.

Clark DB, Taylor CM, Thorpe AJ, Harding RJ, Nicholls ME. 2003. The influence of spatial variability of boundary-layer moisture on tropical continental squall lines. *Q. J. R. Meteorol. Soc.* **129**: 1101–1121.

Clark DB, Taylor CM, Thorpe AJ. 2004. Feedback between the land surface and rainfall at convective length scales. *J. Hydrometeorol.* **5**: 625–639.

Ek MB, Holtslag AAM. 2004. Influence of soil moisture on boundary layer cloud development. *J. Hydrometeorol.* **5**: 86–99.

Eltahir EAB, Gong C. 1996. Dynamics of wet and dry years in West Africa. *J. Climate* **9**: 1030–1042.

Emori S. 1998. The interaction of cumulus convection with soil moisture distribution: An idealized simulation. *J. Geophys. Res.* **103**: 8873–8884.

Findell KL, Eltahir EAB. 2003. Atmospheric controls on soil moisture–boundary layer interactions. Part II: Feedbacks within the continental United States. *J. Hydrometeorol.* **4**: 570–583.

Fink AH, Reiner A. 2003. Spatiotemporal variability of the relation between African easterly waves and West African squall lines in 1998 and 1999. *J. Geophys. Res.* **108**: 4332, DOI:10.1029/2002JD002816

Gash JHC, Kabat P, Monteny BA, Amadou M, Bessemoulin P, Billing H, Blyth EM, de Bruin HAR, Elbers JA, Friborg T, Harrison G, Holwill CJ, Lloyd CR, Lhomme J-P, Moncrieff JB, Puech D, Soegaard H, Taupin JD, Tuzet A, Verhoef A. 1997. The variability of evaporation during the HAPEX-Sahel Intensive Observation Period. *J. Hydrol.* **188–189**: 385–399.

Gruhier C, de Rosnay P, Kerr Y, Mougin E, Ceschia E, Calvet J-C, Richaume P. 2008. Evaluation of AMSR-E soil moisture product based on ground measurements over temperate and semi-arid regions. *Geophys. Res. Lett.* **35**: L10405, DOI:10.1029/2008GL033330

Haase SP, Smith RK. 1989. The numerical simulation of atmospheric gravity currents. Part II. Environments with stable layers. *Geophys. Astrophys. Fluid Dyn.* **46**: 35–51.

Janicot S, Thorncroft CD, Ali A, Asencio N, Berry G, Bock O, Bourles B, Caniaux G, Chauvin F, Deme A, Kergoat L, Lafore J-P, Lavaysse C, Lebel T, Marticorena B, Mounier F, Nedelec P, Redelsperger J-L, Ravegnani F, Reeves CE, Roca R, de Rosnay P, Schlager H, Sultan B, Tomasini M, Ulanovsky A, ACMAD forecasters team. 2008. Large-scale overview of the summer monsoon over West Africa during the AMMA field experiment in 2006. *Annales Geophysicae* **26**: 2569–2595.

Koch SE, Flamant C, Wilson JW, Gentry BM, Jamison BD. 2008. An atmospheric soliton observed with Doppler radar, differential absorption lidar, and a molecular Doppler lidar. *J. Atmos. Oceanic Technol.* **25**: 1267–1287.

Koster RD, Dirmeyer PA, Guo Z, Bonan G, Chan E, Cox P, Gordon CT, Kanae S, Kowalczyk E, Lawrence D, Liu P, Lu C-H, Malyshev S, McAvaney B, Mitchell K, Mocko D, Oki T, Oleson K, Pitman A, Sud YC, Taylor CM, Verseghy D, Vasic R, Xue Y, Yamada T. 2004. Regions of strong coupling between soil moisture and precipitation. *Science* **305**: 1138–1140.

Mohr KI, Zipser EJ. 1996. Mesoscale convective systems defined by their 85-GHz ice scattering signature: Size and intensity comparison over tropical oceans and continents. *Mon. Weather Rev.* **124**: 2417–2437.

Mohr KI, Baker RD, Tao W-K, Famiglietti JS. 2003. The sensitivity of West African convective line water budgets to land cover. *J. Hydrometeorol.* **4**: 62–76.

Negri AJ, Adler RF, Xu L, Surratt J. 2004. The impact of Amazonian deforestation on dry season rainfall. *J. Climate* **17**: 1306–1319.

Owe M, de Jeu R, Holmes T. 2008. Multisensor historical climatology of satellite-derived global land surface moisture. *J. Geophys. Res.* **113**: F01002, DOI:10.1029/2007JF000769

Parker DJ. 2002. The response of CAPE and CIN to tropospheric thermal variations. *Q. J. R. Meteorol. Soc.* **128**: 119–130.

Parker DJ, Burton RR. 2002. The two-dimensional response of a tropical jet to propagating lines of convection. *J. Atmos. Sci.* **59**: 1263–1273.

Parker DJ, Thorncroft CD, Burton RR, Diongue-Niang A. 2005. Analysis of the African easterly jet, using aircraft observations from the JET2000 experiment. *Q. J. R. Meteorol. Soc.* **131**: 1461–1482.

Rabin RM, Stadler S, Wetzel PJ, Stensrud DJ, Gregory M. 1990. Observed effects of landscape variability on convective clouds. *Bull. Am. Meteorol. Soc.* **71**: 272–280.

Ramel R, Gallée H, Messager C. 2006. On the northward shift of the West African monsoon. *Clim. Dyn.* **26**: 429–440.

Redelsperger J-L, Thorncroft CD, Diedhiou A, Lebel T, Parker DJ, Polcher J. 2006. African Monsoon Multidisciplinary Analysis: An international research project and field campaign. *Bull. Am. Meteorol. Soc.* **87**: 1739–1746.

Segal M, Arritt RW. 1992. Nonclassical mesoscale circulations caused by surface sensible heat-flux gradients. *Bull. Am. Meteorol. Soc.* **73**: 1593–1604.

Segal M, Avissar R, McCumber MC, Pielke RA. 1988. Evaluation of vegetation effects on the generation and modification of mesoscale circulations. *J. Atmos. Sci.* **45**: 2268–2292.

Sogalla M, Krüger A, Kerschgens M. 2006. Mesoscale modelling of interactions between rainfall and the land surface in West Africa. *Meteorol. Atmos. Phys.* **91**: 211–221.

Stewart DJ, Taylor CM, Reeves CE, McQuaid JB. 2008. Biogenic nitrogen oxide emissions from soils: Impact on NO_x and ozone over West Africa during AMMA (African Monsoon Multidisciplinary Analysis): Observational study. *Atmos. Chem. Phys.* **8**: 2285–2297.

Taylor CM. 2008. Intraseasonal land–atmosphere coupling in the West African monsoon. *J. Climate* **21**: 6636–6648.

Taylor CM, Ellis RJ. 2006. Satellite detection of soil moisture impacts on convection at the mesoscale. *Geophys. Res. Lett.* **33**: L03404, DOI:10.1029/2005GL025252

Taylor CM, Lebel T. 1998. Observational evidence of persistent convective-scale rainfall patterns. *Mon. Weather Rev.* **126**: 1597–1607.

Taylor CM, Saïd F, Lebel T. 1997. Interactions between the land surface and mesoscale rainfall variability during HAPEX-Sahel. *Mon. Weather Rev.* **125**: 2211–2227.

Taylor CM, Lambin EF, Stephenne N, Harding RJ, Essery RLH. 2002. The influence of land use change on climate in the Sahel. *J. Climate* **15**: 3615–3629.

Taylor CM, Kergoat L, de Rosnay P. 2007a. 'Land surface–atmosphere interactions during the AMMA SOP.' Pp 20–21 in *CLIVAR Exchanges* **12**.

Taylor CM, Parker DJ, Harris PP. 2007b. An observational case study of mesoscale atmospheric circulations induced by soil moisture. *Geophys. Res. Lett.* **34**: L15801, DOI:10.1029/2007GL030572

Texier D, de Noblet N, Braconnot P. 2000. Sensitivity of the African and Asian monsoons to mid-Holocene insolation and data-inferred surface changes. *J. Climate* **13**: 164–181.

Trigo IF, Monteiro IT, Olesen F, Kabsch E. 2008. An assessment of remotely sensed land surface temperature. *J. Geophys. Res.* **113**: D17108, DOI:10.1029/2008JD010035

Wang J, Chagnon FJF, Williams ER, Betts AK, Renno NO, Machado LAT, Bisht G, Knox R, Brase RL. 2009. Impact of deforestation in the Amazon basin on cloud climatology. *Proc. Natl. Acad. Sci. U S A* **106**: 3670–3674.

Xue Y, Shukla J. 1993. The influence of land surface properties on Sahel climate. Part 1. Desertification. *J. Climate* **6**: 2232–2245.

Zheng X, Eltahir EAB, Emanuel KA. 1999. A mechanism relating tropical Atlantic spring sea surface temperature and west African rainfall. *Q. J. R. Meteorol. Soc.* **125**: 1129–1163.

